Orderly Aligned and Highly Luminescent Monodisperse Rare-Earth Orthophosphate Nanocrystals Synthesized by a Limited Anion-Exchange Reaction

Hao-Xin Mai, Ya-Wen Zhang,* Ling-Dong Sun, and Chun-Hua Yan*

Beijing National Laboratory for Molecular Sciences, State Key Lab of Rare Earth Materials Chemistry and Applications & PKU-HKU Joint Lab in Rare Earth Materials and Bioinorganic Chemistry, Peking University, Beijing 100871, China

Received April 20, 2007. Revised Manuscript Received June 25, 2007

High-quality dispersible nanocrystals of $REPO_4$ (RE = La, Eu, Tb, Y, Ho), $LaPO_4$:Ce,Tb, and $REPO_4$:Eu (RE = La,Y) with diverse shapes (nanopolyhedra, quasinanorods, nanorods, and nanowires) were synthesized at temperatures in the range of 180−260 °C in long alkyl-chain solvents (organic acids and amines), via a limited anion-exchange reaction (LAER). Using H_3PO_4 as a precipitator in the LAER, we obtained $REPO_4$ nanocrystals from the precipitation reaction significantly retarded by the strong bonding interactions among the rare earth cations and organic acid ligands. The shape of the nanocrystals can be manipulated to 0D polyhedra, 1D rods, and 1D wires by changing the composition of the solvent and the alkyl-chain length of the capping ligands. The $LaPO_4$:Ce,Tb and $REPO_4$:Eu (RE = La,Y) nanocrystals show intensive green and red emissions under UV excitation, respectively, with quantum yields higher than 40%. Interestingly, the charge-transfer band decided by the RE−O bond distance and the ratio of the I_{610}/I_{590} determined by the symmetries of the Eu^{3+} ions in the host lattice are observed to vary with crystallite size for the differently shaped $REPO_4$:Eu nanocrystals. The highly luminescent nanocrystals can be orderly aligned to form various 2D and 3D nanoarrays on the copper grids by tuning the concentration of the nanocrystal dispersion in cyclohexane, showing their potential in constructing new self-assembled luminescence devices. Moreover, the demonstrated LAER strategy is extendable to the synthesis of many other rare earth salt nanocrystals, such as vanadates and fluorides.

Introduction

The synthesis of high-quality dispersible inorganic nanocrystals (such as metals, II−VI and III−V group semiconductors, and metal oxides) has attracted intensive interest in the fields of chemistry, physics, material science, nanoscience, and nanotechnology.[1] Various wet chemical strategies have been designed and developed so as to obtain such nanocrystals with controlled size, shape, phase, and composition, which not only are recognized for their unique material properties, but also have already acted as the building blocks for the nanodevices composed of 2D and 3D assembles.[2,3] For a given inorganic compound, it still remains a challenge to establish a suitable reaction system for growing the high-quality nanocrystalline products with controlled-size/shape and manipulated self-assembled ability by a green, facile, and economic strategy.[3]

As an important sort of lanthanide inorganic salts, rare-earth (RE) orthophosphates ($REPO_4$) and their nanocrystals have been widely used in the production of luminescence or laser materials, moisture sensors, heat-resistant materials, and nuclear waste disposal.[4] New applications of nanoscale phosphors include transparent luminescence layers or markers, luminescence fillers in transparent matrices, fluorescence resonance energy transfer (FRET) assays, biolabeling, optical

* Corresponding author. Fax: 86-10-6275-4179. E-mail: yan@pku.edu.cn (C.-H.Y.); ywzhang@pku.edu.cn (Y.-W.Z.).

(1) (a) Alivisatos, A. P. *Science* **1996**, *271*, 933. (b) Ahmadi, T. S.; Wang, Z. L.; Green, T. C.; Henglein, A.; El-Sayed, M. A. *Science* **1996**, *272*, 1924. (c) Bruchez, M.; Moronne, M.; Gin, P.; Weiss, S.; Alivisatos, A. P. *Science* **1998**, *281*, 2013. (d) Sun, S. H.; Murray, C. B.; Weller, D.; Folks, L.; Moser, A. *Science* **2000**, *287*, 1989. (e) Shevchenko, E. V.; Talapin, D. V.; Kotov, N. A.; O'Brien, S.; Murray, C. B. *Nature* **2006**, *439*, 55.

(2) (a) Wang, X.; Zhuang, J.; Peng, Q.; Li, Y. D. *Nature* **2005**, *437*, 121. (b) Jun, Y. -W.; Choi, J. -S.; Cheon, J. *Angew. Chem., Int. Ed.* **2006**, *45*, 3414. (c) Xia, Y. N.; Yang, P. D.; Sun, Y. G.; Wu, Y. Y.; Mayers, B.; Gates, B.; Yin, Y. D.; Kim, F.; Yan, H. Q. *Adv. Mater.* **2003**, *15*, 353. (d) Hu, J. T.; Odom, T. W.; Lieber, C. M. *Acc. Chem. Res.* **1999**, *32*, 435. (e) Park, J.; Joo, J.; Kwon, S. -G.; Jang, Y.; Hyeon, T. *Angew. Chem., Int. Ed.* **2007**, *46*, 4630.

(3) (a) Murray, C. B.; Norris, D. J.; Bawendi, M. G. *J. Am. Chem. Soc.* **1993**, *115*, 8706. (b) Li, Y.; Malik, M. A.; O'Brien, P. *J. Am. Chem. Soc.* **2006**, *128*, 16020. (c) Park, J.; An, K.; Hwang, Y.; Park, J.-G.; Noh, H.-J.; Kim, J.-Y.; Park, J.-H.; Hwang, N.-M.; Hyeon, T. *Nat. Mater.* **2004**, *3*, 891. (d) Yu, T.; Joo, J.; Park, Y. -I.; Hyeon, T. *J. Am. Chem. Soc.* **2006**, *128*, 1786. (e) Narayanaswamy, A.; Xu, H. F.; Pradhan, N.; Peng, X. G. *Angew. Chem., Int. Ed.* **2006**, *45*, 5361. (f) Mai, H. X.; Zhang, Y. W.; Si, R.; Yan, Z. G.; Sun, L. D.; You, L. P.; Yan, C. H. *J. Am. Chem. Soc.* **2006**, *128*, 6426. (g) Yin, Y. D.; Alivisatos, A. P. *Nature* **2005**, *437*, 664. (h) Urban, J. J.; Talapin, D. V.; Shevchenko, E. V.; Murray, C. B. *J. Am. Chem. Soc.* **2006**, *128*, 3248. (i) Shevchenko, E. V.; Talapin, D. V.; Murray, C. B.; O'Brien, S. *J. Am. Chem. Soc.* **2006**, *128*, 3620. (j) Si, R.; Zhang, Y. W.; Zhou, H. P.; Sun, L. D.; Yan, C. H. *Chem. Mater.* **2007**, *19*, 18. (k) Zhang, Y. W.; Sun, X.; Si, R.; You, L. P.; Yan, C. H. *J. Am. Chem. Soc.* **2005**, *127*, 3260.

(4) (a) Lehmann, O.; Kompe, K.; Haase, M. *J. Am. Chem. Soc.* **2004**, *126*, 14935. (b) Riwotzki, K.; Meyssamy, H.; Kornowski, A.; Haase, M. *J. Phys. Chem. B* **2000**, *104*, 2824. (c) Meyssamy, H.; Riwotzki, K. *Adv. Mater.* **1999**, *11*, 840. (d) Schuetz, P.; Caruso, F.; *Chem. Mater.* **2002**, *14*, 4509. (e) Nishihama, S.; Hirai, T.; Komasawa, I. *J. Mater. Chem.* **2002**, *12*, 1053.

10.1021/cm071073l CCC: $37.00
Published on Web 08/02/2007

Table 1. Crystal Structures and Morphologies of REX_n Nanocrystals Synthesized at 180−330 °C through the LAER in Oleic Acid (OA), Lauric Acid (LA)/Oleylamine (OM)/1-Octadecene (ODE)

	precursors	solvent	T (°C)	t (h)	structure	morphology	size (nm)
$LaPO_4$	$La(OH)_3$	OA:OM = 1:3	180	5	monoclinic	polyhedron	3.3 ± 0.3[a]
$EuPO_4$	$Eu(NO_3)_3$	OA:OM = 1:3	180	6	monoclinic	polyhedron	4.0 ± 0.3
$TbPO_4$	$Tb(NO_3)_3$	OA:OM = 1:3	180	6	monoclinic	polyhedron	4.1 ± 0.4
		OA:OM = 3:1	180	2	tetragonal	wire	$(1.5 \pm 0.1) \times (40-70)$
YPO_4	$Y(NO_3)_3$	OA:OM = 3:1	180	2	tetragonal	wire	$(1.6 \pm 0.1) \times (100-200)$
$HoPO_4$	$Ho(NO_3)_3$	OA:OM = 3:1	180	2	tetragonal	wire	$(1.5 \pm 0.1) \times (100-200)$
$LaPO_4$:Ce,Tb	$La(NO_3)_3$	OA:OM = 1:3	180	5	monoclinic	polyhedron	2.9 ± 0.2
	$Ce(NO_3)_3$	OA:OM = 2:2	180	5	monoclinic	quasirod	$(7.7 \pm 0.6) \times (2.7 \pm 0.3)$
	$Tb(NO_3)_3$	OA:OM = 4:0	180	5	monoclinic	rod	$(6.9 \pm 1.1) \times (30-50)$
	H_3PO_4	LA:OM =1:3	180	5	monoclinic	wormlike wire	$(2.8 \pm 0.2) \times (10-40)$
$LaPO_4$:Eu	$La(NO_3)_3$	OA:OM = 1:3	180	5	monoclinic	polyhedron	3.3 ± 0.3
	$Eu(NO_3)_3$	OA:OM = 4:0	180	5	monoclinic	rod	$(6.9 \pm 1.1) \times (50-100)$
YPO_4:Eu	$Y(NO_3)_3$	OA:OM = 2:2	180	2	tetragonal	polyhedron	20−50
	$Eu(NO_3)_3$	OA:OM = 3:1	180	2	tetragonal	wire	$(1.4 \pm 0.1) \times (70-200)$
α-$NaYF_4$	$Y(OH)_3$ NaF	OA:OM:ODE = 1:1:2	260	1	cubic	polydedron	13.2 ± 0.8
β-$NaYF_4$	α-$NaYF_4$ NaF	OA:ODE = 1:1	330	0.5	hexagonal	hexagon	218 ± 15

[a] The standard deviation statistic from at least 100 particles.

imaging, or phototherapy.[4,5] It is widely accepted that, to obtain luminescent nanocrystals with high quantum yield (QY), high-quality nanocrystals with fewer lattice defects and surface damages must be obtained, and special attention should be paid to the surface structures of the nanocrystals (including the surface site of the luminescent ions and the surface bonding of the capping ligands). In recent years, several methods have been developed to synthesize $REPO_4$ nanocrystals by a number of research groups.[6] Various $REPO_4$ nanostructures (such as 1D wires and rods) were hydrothermally prepared by the groups of Xu,[6a] Yan,[6b] and Li.[6c] Haase et al. obtained $REPO_4$ nanocrystal dispersions with good optical properties with a high-boiling-solvent technique.[6d,e] Buhler et al. fabricated luminescent $LaPO_4$:Ce,Tb nanoparticles with high quantum yield, using a microwave-assisted synthesis method with some ionic liquids as the reaction media.[6f]

In this paper, we report the synthesis of orderly aligned and highly luminescent monodisperse nanocrystals of $REPO_4$ (RE = La, Eu, Tb, Y, Ho), $LaPO_4$:Ce,Tb, and $REPO_4$:Eu (RE = La,Y) with diverse shapes (polyhedra, rods, and wires), by a limited anion-exchange reaction (LAER) in solution phase. The as-synthesized doped $REPO_4$ nanopolyhedra, quasinanorods, nanorods, and nanowires display intensive green and red emissions with high QY under UV excitations. In particular, the differently sized $REPO_4$:Eu nanocrystals show interesting photoluminescence (PL) properties. Moreover, because of their intriguing size uniformity, the nanocrystals can be easily aligned to form 2D and 3D superlattice on carbon-coated copper grids via spontaneous organization.

(5) (a) Pellegrino, T.; Kudera, S.; Liedl, T.; Javier, A. M.; Manna, L.; Parak, W. *Small* **2005**, *1*, 48. (b) Zhang, C. Y.; Yeh, H. C.; Kuroki, M. T.; Wang, T. H. *Nat. Mater.* **2005**, *4*, 826. (c) Kim, S.; Lim, Y. T.; Soltesz, E. G.; DeGrand, A. M.; Lee, J.; Nakayama, A.; Parker, J. A.; Mihaljevic, T.; Laurence, R. G.; Dor, D. M.; Cohn, L. H.; Bawendi, M. G.; Frangioni, J. V. *Nat. Biotechnol.* **2003**, *22*, 93. (d) Dubertret, B.; Skourides, P.; Norris, D. J.; Noireaux, V.; Brivanloue, A. H.; Libchaber, A. *Science* **2002**, *298*, 1759. (e) Shipway, A. N.; Katz, E.; Willner, I. *ChemPhysChem* **2000**, *1*, 19.

(6) (a) Fang, Y. P.; Xu, A. W.; Song, R. Q.; Zhang, H. X.; You, L. P.; Yu, J. C.; Liu, H. Q. *J. Am. Chem. Soc.* **2003**, *125*, 16025. (b) Zhang, Y. W.; Yan, Z. G.; You, L. P.; Si, R.; Yan, C. H. *Eur. J. Inorg. Chem.* **2003**, 4099. (c) Yan, R. X.; Sun, X. M.; Wang, X.; Peng, Q.; Li, Y. D. *Chem.—Eur. J.* **2005**, *11*, 2187. (d) Riwotzki, K.; Meyssamy, H.; Schnablegger, H.; Kornowski, A.; Haase, M. *Angew. Chem., Int. Ed.* **2001**, *40*, 573. (e) Kompe, K.; Borchert, H.; Storz, J.; Lobo, A.; Adam, S.; Moller, T.; Haase, M. *Angew. Chem., Int. Ed.* **2003**, *42*, 5513. (f) Buhler, G.; Feldmann, C. *Angew. Chem., Int. Ed.* **2006**, *45*, 4864.

Experimental Section

Materials. Oleic acid (OA, Aldrich), oleylamine (OM, Acros), 1-octadecene (ODE, Acros), lauric acid (LA, Acros), decanoic acid (DA, Beijing Chem. Corp. China), heptanoic acid (HA, Beijing Chem. Corp. China), ethanol (AR), cyclohexane (AR), and toluene (AR) were used as received without further purification.

Synthesis of $REPO_4$ Nanocrystals: Typically, 1 mmol of $RE(OH)_3$ (or $RE(NO_3)_3$, AR) was added to 10 mmol of OA in a three-necked flask at room temperature. The slurry was heated to 140 °C to remove water and oxygen for 30 min, and thus to form an optically transparent solution. Then, a suitable amount of OA and OM (Table 1) was added in the system and again the solution was heated to 140 °C to remove water and oxygen for 30 min. After that, 1 mmol of H_3PO_4 dispersed in 3 mmol of ODE was injected into the solution at 180 °C under an Ar atmosphere. The resulting mixture was kept at 180 °C for 2−6 h to give a slightly turbid solution. Then, an excess amount of ethanol was poured into the solution at room temperature. The resultant mixture was centrifugally separated and the products were collected. The as-precipitated nanocrystals were washed several times with ethanol and then dried in air at 70 °C overnight. The yields of all the obtained nanocrystals were around 80%. The as-prepared nanocrystals could be easily redispersed in various nonpolar organic solvents, such as cyclohexane and toluene.

Synthesis of $LaPO_4$:Ce,Tb Nanocrystals. The synthetic procedure for the $LaPO_4$:Ce,Tb nanocrystals was the same as that used for the synthesis of the $LaPO_4$ nanopolyhedra, except that 0.4 mmol of $La(NO_3)_3$, 0.45 mmol of $Ce(NO_3)_3$, and 0.15 mmol of $Tb(NO_3)_3$ were used as the precursors in OA/OM (Table 1).

Synthesis of $LaPO_4$:Eu Nanocrystals. The synthetic procedure for the $LaPO_4$:Eu nanocrystals was the same as that used for the synthesis of the $LaPO_4$ nanopolyhedra, except that 0.95 mmol of $La(NO_3)_3$ and 0.05 mmol of $Eu(NO_3)_3$ were used as the precursors in OA/OM (Table 1).

Synthesis of YPO_4:Eu Nanocrystals. The synthetic procedure for the YPO_4:Eu nanocrystals was the same as that used for the synthesis of the YPO_4 nanopolyhedra, except that 0.95 mmol of $Y(NO_3)_3$ and 0.05 mmol of $Eu(NO_3)_3$ were used as the precursors in OA/OM (Table 1).

Synthesis of YVO_4 Nanocrystals. The synthetic procedure was the same as that used for the synthesis of the $REPO_4$ nanocrystals,

except that 1 mmol of $Na_3VO_4 \cdot 12H_2O$ (AR) dissolved in 1 mmol of acetic acid (AR) was added under OA:OM = 1:6 for a reaction at 220 °C for 1 h. The yield of the nanocrystals was ~80% (Table 1).

Synthesis of α-$NaYF_4$ Nanocrystals. The synthetic procedure was the same as that used for the synthesis of the $REPO_4$ nanocrystals, except that 2 mmol of NaF (AR) was added under OA:OM:ODE = 1:1:2 for a reaction at 260 °C for 1 h. The yield of the nanocrystals was ~60% (Table 1).

Synthesis of *β*-$NaYF_4$ Nanocrystals. The synthetic procedure was the same as that used for the synthesis of the α-$NaYF_4$ nanocrystals, except that quantitative NaF and the as-prepared α-$NaYF_4$ nanocrystals were taken as the precursors and added into 40 mmol of OA/ODE at the ratio of 1:1 in a three-necked flask at room temperature (Table 1).

Instrumentation. Powder X-ray diffraction (XRD) patterns of the dried powders were recorded on a Rigaku D/MAX-2000 diffractometer (Japan) with a slit of 1/2 ° at a scanning rate of 2° min^{-1}, using Cu-K_α radiation (λ = 1.5406 Å). The lattice parameters were calculated with the least-squares method. Samples for transmission electron microscopy (TEM) analysis were prepared by drying a drop of nanocrystal dispersion in cyclohexane on amorphous carbon-coated copper grids. Particle sizes and shapes were examined by a TEM (200CX, JEOL, Japan) operated at 160 kV. High-resolution TEM (HRTEM) characterization was performed with a Philips Tecnai F30 FEG-TEM (USA) operated at 300 kV. FTIR spectra of the samples (prepared by directly depositing some of the product solutions in cyclohexane onto a KBr wafer) were obtained with a Nicolet Magna 750 spectrophotometer. Room-temperature fluorescence spectra were recorded on a Hitachi F-4500 spectrophotometer equipped with a 150 W Xe-arc lamp at a fixed bandpass of 0.2 nm with the same instrument parameters (2.5 nm for excitation slit, 2.5 nm for emission slit, and 700 V for PMT voltage), with the samples of $LaPO_4$:Yb,Tb and $REPO_4$:Eu nanocrystals dispersed in cyclohexane at a concentration of 2 wt %.

Results and Discussion

1. Characteristics of $REPO_4$ Nanocrystals. *Undoped $REPO_4$.* Panels a, c, and d of Figure S1 in the Supporting Information show the XRD patterns of the undoped $REPO_4$ (RE = La, Eu, Y) nanocrystals. $LaPO_4$ and $EuPO_4$ nanocrystals are of pure monoclinic phases (monazite type, space group $P2_1/n$). The calculated lattice constants are as follows: a = 6.88 (5) Å, b = 7.09 (3) Å, c = 6.56 (1) Å, and β = 103.1° (1) for $LaPO_4$, and a = 6.68 (2) Å, b = 6.83 (3) Å, c = 6.33 (2) Å, and β = 103.5° (3) for $EuPO_4$ (see panels a and c of Figure S1 and Table S1 in the Supporting Information). YPO_4 and $HoPO_4$ nanocrystals are in a tetragonal structure (zircon type, space group $I4_1/amd$), with the lattice constant of a = 6.97 (2) Å and c = 5.97 (3) Å, and a = 6.95 (3) Å and c = 5.99 (3) Å, respectively (Figure S1d and Table S1 in the Supporting Information). $TbPO_4$ nanocrystals appear in two different polymorphs. The $TbPO_4$ nanopolyhedra were of monazite type with the lattice constant of a = 6.63 (5) Å, b = 6.83 (4) Å, c = 6.33 (2) Å, and β = 103.7° (2) (see Figure S1c and Table S1 in the Supporting Information), whereas the $TbPO_4$ nanowires were of zircon type with the lattice constant of a = 6.94 (5) Å and c = 6.01 (1) Å (see Figure S1d and Table S1 in the Supporting Information). The atomic ratios of metals in the nanocrystals were determined by energy-dispersive X-ray analysis (EDAX), which confirmed the formation of stoichiometric $REPO_4$ (see Figure S1b in the Supporting Information).

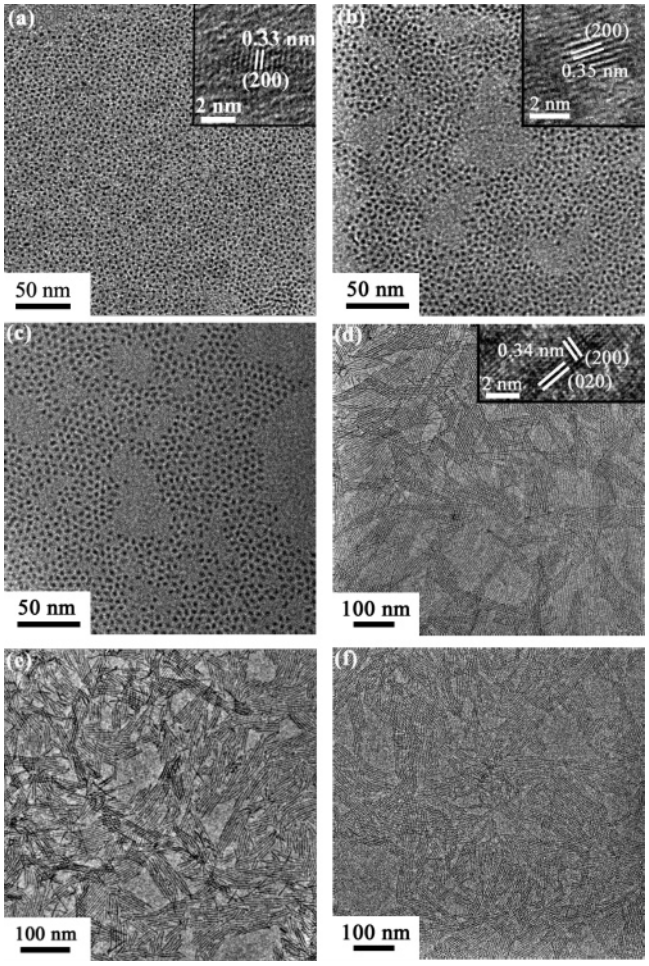

Figure 1. TEM and HRTEM images (insets) of (a) $LaPO_4$ polyhedra and (b) $EuPO_4$ polyhedra. (c) TEM image of $TbPO_4$ polyhedra. (d) TEM and HRTEM images (inset) of YPO_4 nanowires. TEM images of (e) $TbPO_4$ and (f) $HoPO_4$ nanowires.

The TEM and HRTEM images shown in Figure 1 demonstrate that all the as-obtained $REPO_4$ nanocrystals are of single-crystalline nature and display high crystallite size uniformity. Figure 1a−c reveal the formation of 3.3 nm $LaPO_4$, 4.0 nm $EuPO_4$, and 4.1 nm $TbPO_4$ nanopolyhedra, respectively. From the HRTEM insets in images a and b of Figure 1, the (200) lattice fringes are observable for $LaPO_4$ and $EuPO_4$, respectively. Panels 1d−f of Figure 1 display the order alignment of the ultra-fine YPO_4, $TbPO_4$, and $HoPO_4$ nanowires, respectively. Interestingly, the nanowires are longer than 100 nm and show a highly uniform width of 1.6 nm.[3d] Such a uniform 1D nanostructure has not been reported for zircon-type $REPO_4$ before.[6] The preferred growth direction of the nanowires is along [100] (a-axis).

Doped $REPO_4$. The XRD patterns shown in Figures S2a, S3a, and S3b in the Supporting Information reveal the formation of monoclinic $LaPO_4$:Ce,Tb and $LaPO_4$:Eu nanocrystals and tetragonal YPO_4:Eu nanocrystals.[6d,e] The distinct shrinkage of the calculated lattice constants from $LaPO_4$ to $LaPO_4$:Ce,Tb confirms the formation of homogeneous $LaPO_4$:Ce,Tb solid solution (see Table S1 in the Supporting Information). Noticeably, the broadening of the reflections

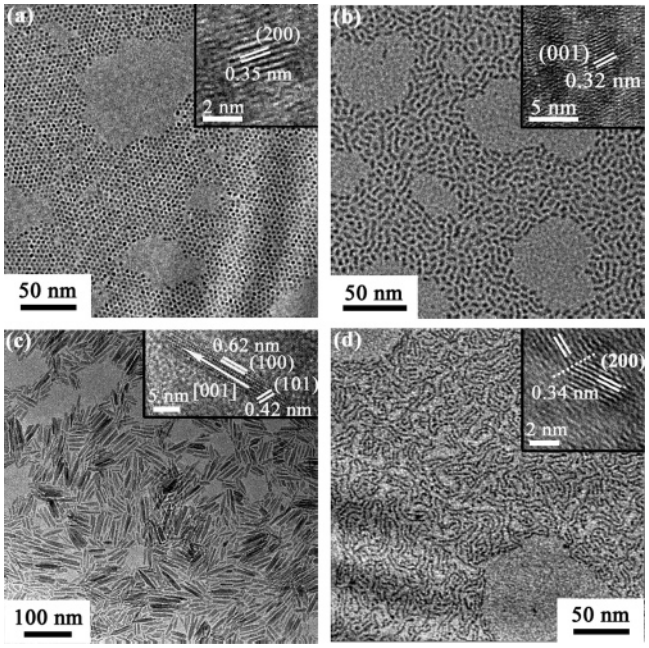

Figure 2. TEM and HRTEM images (inset) of the $LaPO_4$:Ce,Tb (a) nanopolyhedra (0.01 mol L^{-1}), (b) quasi-nanorods, (c) nanorods, and (d) wormlike nanowires (highlighted: the twined (200) plane).

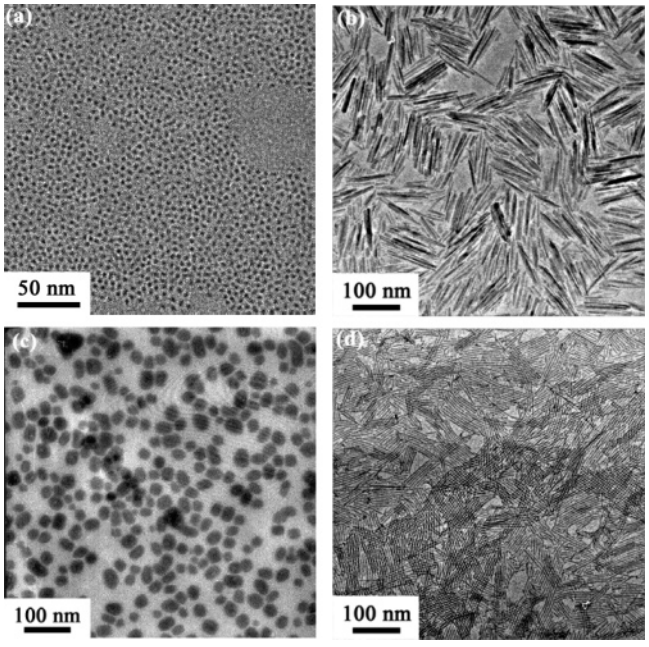

Figure 3. TEM images of $LaPO_4$:Eu (a) nanopolyhedra (0.01 mol L^{-1}) and (b) nanorods and YPO_4:Eu (c) nanopolyhedra and (d) nanowires.

Scheme 1. Schematic Illustration of the LAER Strategy for the Synthesis of $REPO_4$ Nanocrystals

ascribed to the $LaPO_4$:Ce,Tb and $LaPO_4$:Eu polyhedra distinctly indicates their nanocrystalline nature (see the Supporting Information, panels a and b in Figure S2). The sharper reflections for the $LaPO_4$:Ce,Tb wires, rods, and quasirods and the $LaPO_4$:Eu rods imply their larger sizes as compared with the former two samples (see panels a and b in Figure S3 of the Supporting Information). In particular, for YPO_4:Eu nanowires, the much intenser and sharper (200) peak reveals that they preferably grow along [100] (see the Supporting Information, Figure S3b).

Figure 2 depicts the diverse morphologies of typical doped $REPO_4$ nanocrystals. As shown in the inset of Figure 2a, the 2.9 nm $LaPO_4$:Ce,Tb polyhedra are single-crystalline, showing the interplanar spacing of 0.35 nm ascribed to the (200) crystal plane of monoclinic $LaPO_4$:Ce,Tb. The morphologies of the doped $REPO_4$ nanocrystals can be controlled through changing the components of the solvents. With increasing the amount of OA in the solution, the $LaPO_4$:Ce,Tb nanocrystals grow more anisotropically. $(2.7 \pm 0.3) \times (7.7 \pm 0.6)$ nm $LaPO_4$:Ce,Tb quasirods are formed (Figure 2b) under OA:OM = 1:1, whereas (6.9 ± 1.1) nm $\times$ (30−50) nm $LaPO_4$:Ce,Tb nanorods are obtained with pure OA as the solvent (Figure 2c). The HRTEM images inserted in images b and c of Figure 2 disclose that the 1D growth direction of the quasirods and rods are both along [001]. As OA is replaced with lauric acid (LA) (Table 1), $LaPO_4$:Ce,Tb wormlike nanowires (Figure 2d) are obtained, which exhibited 2D ordering on the TEM grids. From the HRTEM image inserted in Figure 2d, it is noted that the $LaPO_4$:Ce,Tb wires are highly crystallized with the interplanar spacing of 0.34 nm corresponding to the (200) crystal plane. The appearance of a twined (200) plane on the HRTEM image (as marked by the dotted line) indicates that the wires may be formed by an oriented attachment aggregation (Figure 2d).[3g] This synthesis is similar to the synthesis of other $REPO_4$. When the ratio of OA/OM is low, (3.3 ± 0.3) nm $LaPO_4$:Eu nanopolyhedra and nonuniform YPO_4:Eu nanoparticles are synthesized (images a and c in Figure 3). With an increasing amount of OA, (6.9 ± 1.1) nm $\times$ (50−100) nm $LaPO_4$:Eu nanorods and (1.4 ± 0.1) nm $\times$ (70−200) nm YPO_4:Eu nanowires are obtained (images b and d in Figure 3).

2. Reaction Pathway for the Formation of $REPO_4$ Nanocrystals. *Evidence of the Limited Anion-Exchange Reaction.* The LAER strategy proposed in this work is depicted in Scheme 1, which involves two crucial steps: (1) the rare-earth source compound (REL_3, L = OH^-, NO_3^-, or Ac^-) is fully dissolved in a long-chain fatty acid (RCOOH) solution upon heating to a certain temperature, in which L^- ions are substituted by $RCOO^-$ to form $REL_{3-x}(RCOO)_x$; (2) an anion-exchange reaction between PO_4^{3-}, provided by an anion source (PO_4^{3-}, dissolved in the long alkyl-chain solvents), and $RCOO^-/L^-$ will take place at a further elevated temperature, resulting in the formation of $REPO_4$. Under this condition, the strong coordination between RE cations and carboxyl groups of the fatty acid ligands greatly limits the anion exchange reaction, thereby achieving a well-maintained balance between nucleation and growth stages. As a result, monodisperse $REPO_4$ nanocrystals can be obtained from the so-called LAER. As the surfaces of the nanocrystals are well-coated by long-chain fatty acids, the as-obtained $REPO_4$ nanocrystals tend to be orderly aligned on the copper grids

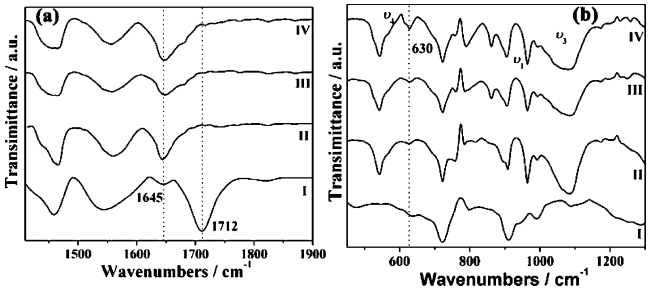

Figure 4. FTIR spectra of the reaction mixture taken at different stages in the (a) 2000−1400 cm^{-1} spectrum window and (b) 1300−450 cm^{-1} spectrum window . (I) $La(OH)_3$ dissolved in OA; (II) H_3PO_4 injected into the mixture of OM/OA; (III) the reaction after a 1 h duration; and (IV) the reaction after a 2 h duration.

to form superlattices via self-assembly due to the hydrophobic nature of the long alkyl chain of the capping ligands.

The process of the LAER strategy can be illustrated in detail via the FTIR spectra. Figure 4 showed the FTIR spectra of the reaction mixture taken at different stages,[7,8] using the synthesis of $LaPO_4$ nanocrystals as an example. No $P_2O_7^{4-}$ was formed in the whole process.[8] When $La(OH)_3$ dissolved in OA and the solution became clear, the FTIR spectra (Figure 4a) show that, at this time, the $-COO^-$ asymmetric vibration (1645 cm^{-1}) was clearly visible, although the carbonyl peak of $-COOH$ (1712 cm^{-1}) was strong. This result implied that the OA ligands substituted OH^- anions and chelated with La^{3+} cations.[2e,3c,j] When 30 mmol of OM was added, the carbonyl peak of $-COOH$ disappeared and the $-COO^-$ asymmetric vibration became stronger, which meant that all deassociated OA molecules were reacted with OM (Figures 4a and S4a). As some H_3PO_4 in ODE were injected into the reaction medium, the vibrations within 1400−2000 cm^{-1} showed no obvious changes, but the vibration of PO_4^{3-} was found within 1300−450 cm^{-1} (Figure 4b).[8] It seemed that H_3PO_4 would first react with OM and formed organic ammonium phosphates. As seen from Figure S4b, no H_3PO_4 vibrations but only those of PO_4^{3-} could be observed when H_3PO_4 was added into a solution containing an excessive amount of OM. The anion-exchange reaction between PO_4^{3-} and OA anions was then greatly limited predominately because of the strong chelation between OA and RE^{3+}. Figure 4b showed that the typical vibration of $LaPO_4$ at 630 cm^{-1} gradually became strong with extending the reaction time, indicating that the growth of the $LaPO_4$ nanocrystals was significantly restrained.[7] Therefore, monodisperse $LaPO_4$ nanocrystals were obtained.

Extension of the LAER. The present LAER strategy was extendable to the synthesis of monodisperse and single-crystalline nanocrystals of other RE salt compounds (Figures 5 and S5 and Table S1). For instance, when VO_4^{3-} served as the anion source, orderly aligned tetragonal YVO_4 nanocrystals (space group $I4_1/amd$) were obtained. Figure 5a reveals that the (4.9 ± 0.5) nm × (6.6 ± 0.4) nm YVO_4 cubes are enclosed by {100} and {001} facets. As NaF was

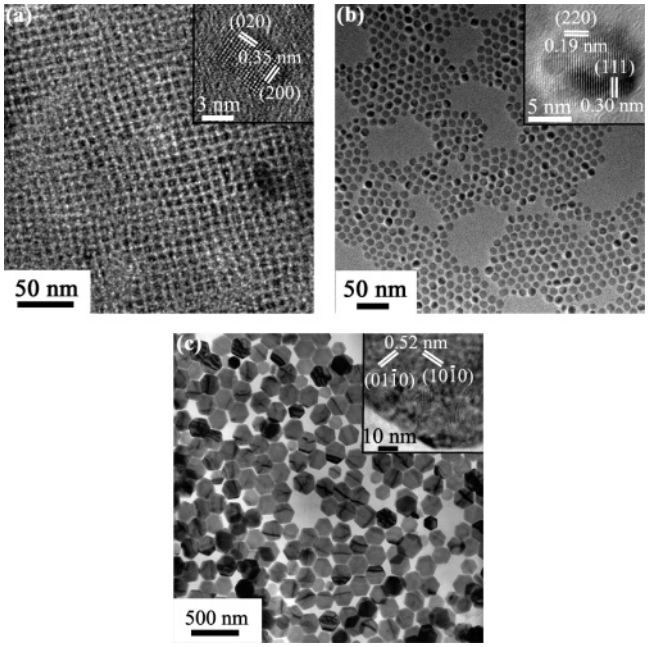

Figure 5. TEM and HRTEM images (insets) of (a) YVO_4 nanocubes, (b) α-$NaYF_4$ nanopolyhedra, (c) and β-$NaYF_4$ hexagonal plates.

adopted as the F^- source, both cubic (α-phase) and hexagonal (β-phase) $NaYF_4$ were obtained (space group: $Fm\bar{3}m$ for α-$NaYF_4$ and $P\bar{6}$ for β-$NaYF_4$). Compared with our previous work,[3f] this LAER strategy adopted nontoxic and more readily available chemicals such as hydrates, nitrates, and acetates as RE sources to synthesize high-quality $NaYF_4$ nanocrystals. Figure 5b shows that the 13.2 nm α-$NaYF_4$ nanocrystals are of polyhedron shape, and the interplanar spacing of 0.31 and 0.19 nm are obvious, which correspond to the (111) and (220) planes of α-$NaYF_4$, respectively. Figure 5c shows the formation of 218 nm × 100 nm β-$NaYF_4$ hexagonal plates enclosed by {10$\bar{1}$0} and {0001} facets.

3. Phase Control and Shape Evolution of $REPO_4$ Nanocrystals. *Phase Control.* As is well-known, anhydrous $REPO_4$ has two polymorphs at ambient pressure: for the light and middle rare-earth ions, $REPO_4$ crystallize in the monazite type structure (monoclinic), whereas for the heavy rare-earth ions, $REPO_4$ adopt zircon type structure (tetragonal).[6] In the present work, the case is similar, but dependent upon the ratio of OA to OM adopted in the synthesis. For the light and middle RE^{3+} (RE = La−Gd), we obtained monoclinic $REPO_4$, regardless of the ratio of OA to OM (Table 1), whereas for the heavy RE^{3+} (RE = Ho−Lu, Y), we obtained tetragonal $REPO_4$ only under OA/OM >1. For Tb^{3+} and Dy^{3+}, we can selectively obtain monoclinic or tetragonal nanocrystals by turning the OA/OM ratio. Monoclinic phase is obtained when OA/OM is around 1:1, whereas the tetragonal phase is formed under OA/OM > 3:2. It is worth pointing out that, for the rare earths from Tb to Lu including Y, no $REPO_4$ nanocrystals can be obtained even after 24 h reaction under OA/OM < 1, presumably as a result of the significantly enhanced solubility of their compounds under this condition along the rare-earth series.[6,8b]

Shape Evolution. As shown recently, the anisotropic nature of building blocks in crystal structure of nanocrystals and accelerated dissolution/recrystallization process in solutions

(7) (a) Chen, Y. F.; Kim, M.; Lian, G. D.; Johnson, M. B.; Peng, X. G. *J. Am. Chem. Soc.* **2005**, *127*, 13331. (b) Narayanaswamy, A.; Xu, H. F.; Pradhan, N.; Kim, M.; Peng, X. G. *J. Am. Chem. Soc.* **2006**, *128*, 10310.

(8) (a) KIijkowska, R.; Cholewka, E.; Duszak, B. *J. Mater. Sci.* **2003**, *38*, 223. (b) KIijkowska, R. *J. Mater. Sci.* **2003**, *38*, 229.

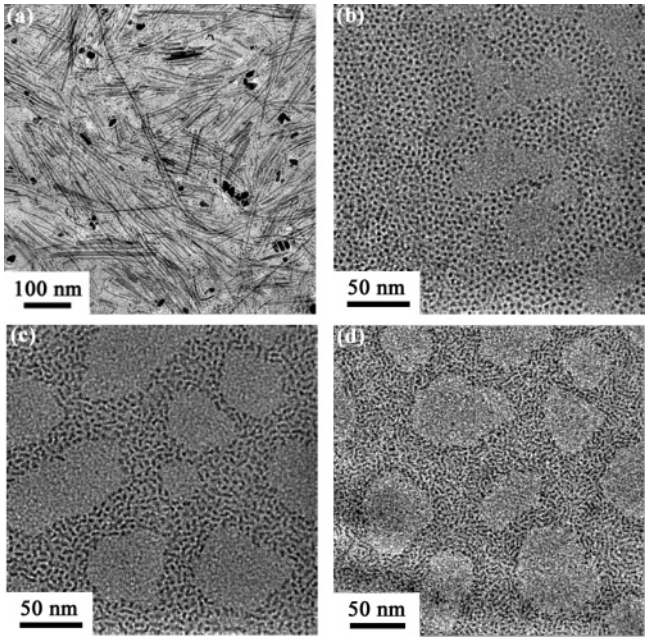

Figure 6. (a) TEM image of the products obtained by using $LaPO_4$:Ce,Tb polyhedra as the precursors in OA. TEM images of $LaPO_4$:Ce,Tb obtained under LA:OM = 1:3 at 180 °C for (b) 1, (c) 3, and (d) 4 h.

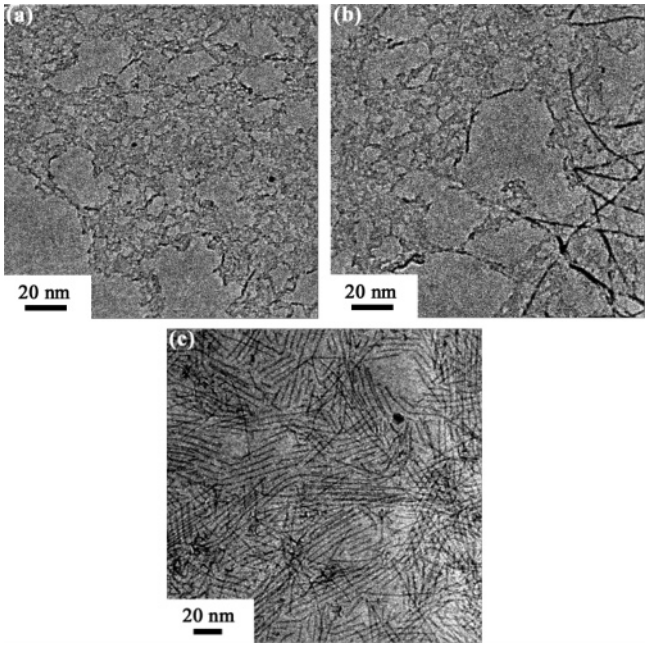

Figure 7. TEM images of YPO_4:Eu obtained under OA:OM = 3:1 at 180 °C for (a) 0, (b) 15, and (c) 30 min.

are two major driving forces for 1D growth of the $REPO_4$ nanostructures.[6a−c] To explain the formation of 1D monoclinic $REPO_4$ nanomaterials obtained in the present work, we take $LaPO_4$:Ce,Tb as an example and suggest that the speed of the dissolution/recrystallization for forming the anisotropic monazite $REPO_4$ nanocrystals should be raised with increasing the amount of OA. In the experiments, $LaPO_4$:Ce,Tb nanopolyhedra (obtained in the solution of OA:OM = 1:3, Figure 2a) were used as the precursors and underwent further growth in the pure OA solution at 180 °C. After 5 h, the mixture of $LaPO_4$:Ce,Tb nanowires and nanopolyhedra was obtained (Figure 6a). Because no other RE^{3+} and PO_4^{3-} sources existed in the stock solution, the $LaPO_4$:Ce,Tb monomers came from the $LaPO_4$:Ce,Tb nanopolyhedra dissolved in OA. Therefore, it is believed that the high OA/OM ratio leads to a high concentration of $LaPO_4$:Ce,Tb monomers and thus a high growth rate of the $LaPO_4$:Ce,Tb nanocrystals in the solution. Under this condition, the 1D growth was significantly promoted, and thus the shape evolution from 0D nanopolyhedra to 1D nanorods was observed (Figures 2a and 3a). Moreover, the aspect ratio of the $REPO_4$ nanorods seemed to increase along the rare-earth series. For instance, the aspect ratio increases from 8.7 to 14 for $LaPO_4$ nanorods ((60−100) nm × (6.9 ± 1.1) nm), to 8.9−13 for $NdPO_4$ nanorods ((40−60) nm × (4.5 ± 0.8) nm), to 15−22 for $EuPO_4$ nanorods ((40−60) nm × (2.7 ± 0.5) nm) (see Figure S6 in the Supporting Information).

When OA was replaced by the fatty acids with shorter alkyl chain, the acidity of the solution was likely increased; therefore, the speed of the dissolution/recrystallization and the 1D growth tendency of the monoclinic $REPO_4$ nanocrystals were increased. Figure 6b−d displays the $LaPO_4$:Ce,Tb nanocrystals growing under LA:OM = 1:3 at 180 °C for 1, 3, and 4 h, respectively. Only nanopolyhedra were formed with the reaction time of 1 h (Figure 6b), just like the case of the synthesis under OA:OM = 1:3. For the shortened alkyl chain from OA to LA, the steric hindrance of the carboxylic ligands accessing to the nanocrystal surfaces was reduced, so that the limited anion exchange was gradually promoted, and the aggregation tendency for $LaPO_4$:Ce,Tb nanoparticles by oriented attachment was enhanced.[3g] As a result, short $LaPO_4$:Ce,Tb nanowires were formed with a longer reaction time of 3 h (Figure 6c). With further prolonging the reaction time, wormlike $LaPO_4$:Ce,Tb nanowires were obtained with the increased aspect ratio (Figures 6d and 2d). However, when OA was replaced by decanoic acid (DA) and heptanoic acid (HA), only severely aggregated and ill-shaped rods and polyhedra were obtained, respectively (see Figures S7 in the Supporting Information). This result strongly demonstrated that the steric hindrance decreased with further shortening the alkyl chain, leading to the aggregation of nanocrystals.

The case was similar to the synthesis of tetragonal $REPO_4$ (RE = Ho−Lu, Y). Taking YPO_4:Eu as an example, only some gels along with few nanoparticles were found as soon as H_3PO_4 was injected into the solution (Figure 7a). Then, some nanowires in the size of 1.5 nm × (20−50) nm were seen after the reaction for 15 min (Figure 7b). After 30 min, a great amount of YPO_4:Eu nanowires appeared (Figure 7c). Interestingly, we found that, with extending the reaction time, the nanowires grew longer and longer in an unaltered width resulting in the formation of ultrathin YPO_4:Eu nanowires after 2 h (Figure 3d). We believed that these YPO_4:Eu nanowires in subnanometer range were formed because of the anisotropic structure of tetragonal YPO_4:Eu, the accelerated dissolution/recrystallization for the nanoparticles (OA:OM = 3:1), and the intense bonding of OA on some specific facets (Figure 3d). When the dissolution/recrystallization process was weakened with reducing the OA/OM ratio to 1, only nonuniform nanoparticles were formed (Figure 3c). When the ratio of OA/OM was less than 1, YPO_4:Eu nuclei were hardly formed because of the significantly restricted precipitation reaction between the PO_4^{3-} and RE^{3+} ion, which are caused by the combined action of the relatively high

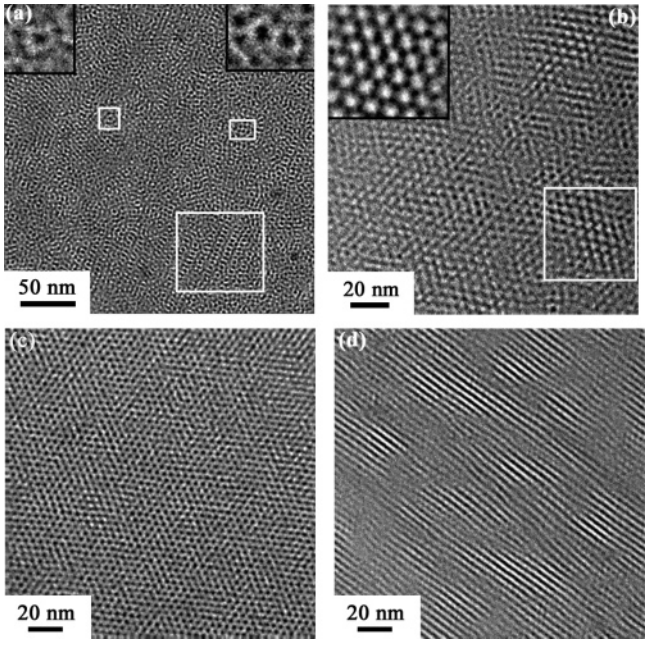

Figure 8. TEM images of $LaPO_4$:Ce,Tb nanopolyhedra deposited from different dispersion concentrations: (a) 0.025 mol L^{-1} (inset, left, wheel-like nanoarray with one core; right, with two cores, taken from the left and right highlighted section, respectively), (b) 0.015 mol L^{-1} (inset, taken from the highlighted section). (c) TEM image of $LaPO_4$:Eu nanopolyhedra deposited from 0.015 mol L^{-1} colloid solution. (d) TEM image of YPO_4:Eu nanowires as-deposited from five drops of 0.005 mol L^{-1} colloid solution.

solubility of $REPO_4$ compounds of heavy rare earths and the increased coordination interaction of the $RCOO^-$ ligands.[6,8] When coming to the $TbPO_4$ and $DyPO_4$, the growth of the nanocrystals followed the monoclinic $REPO_4$ when the ratio of OA/OM was 1, whereas it behaved as the tetragonal $REPO_4$ when the ratio of OA/OM was higher than 3:2. Therefore, uniform nanopolyhedra were obtained under OA/OM = 1 (Figure 1c), and ultrafine nanowires were obtained under OA/OM = 1.5 (Figure 1e).

4. Self-Assembled Behavior of $REPO_4$ Nanocrystals. The ability to form highly ordered and densely packed nanocrystal assemblies is important toward generating advanced materials for a number of technological applications and physical measurements.[1e,3h,i] In particular, it is still a challenge to obtain various self-assembled patterns of nanocrystals in long length scales by simple means. In our previous work, various self-assembled nanoarrays of rare earth oxides and fluorides can be fabricated by manipulating the evaporation and the polarity of the solution.[3j,k] For the present $REPO_4$ nanocrystals, because of their high size uniformity, they can form self-assembled superlattices on the TEM grids. For example, various self-assembled nanoarrays of $LaPO_4$:Ce,Tb nanopolyhedra on the TEM grid could be obtained by varying the concentration of the $REPO_4$ colloidal solution. When the nanocrystal concentration was 0.05 mol L^{-1}, only severely aggregated nanoparticles were found. With diluting the solution, the arrangement of the polyhedra became partially ordered. When the nanocrystal concentration was diluted to 0.025 mol L^{-1}, lots of wheel-like nanoarrays composed of the polyhedra were observed on the grid, which have one or several cores (highlighted sections and insets in Figure 8a, left and right). Some of the wheels further assembled as a line (highlighted section in Figure 8a, lower). A highly ordered hexagonally close-packed (*hcp*) 3D superlattice was found on the TEM grid when the concentration of the solution was 0.015 mol L^{-1} (Figures 8b and S8). This well-ordered *hcp* superlattice still remained, with a length beyond 1 μm (see Figure S9 in the Supporting Information), and in some part of the TEM grid, some hexagonal arrangements were found (highlighted section and inset in Figure 8b). When the solution was diluted to 0.01 mol L^{-1}, the arrangement of the polyhedra became a monolayer and much blank of the grid were seen in Figure 2a. The strategy of manipulating the self-assembly behavior of the $LaPO_4$:Ce,Tb nanopolyhedra can be extended to the controlled formation of $LaPO_4$:Eu and other $REPO_4$ nanoarrays (see Figure S9 in the Supporting Information). When the concentration of the $REPO_4$ nanopolyhedra solution was about 0.015 mol L^{-1}, 3D superlattice could also been found on the TEM grid (Figure 8c). For YPO_4:Eu nanowires, 3D superlattice could be obtained by depositing the diluted solution on the TEM grid several drops (Figure 8d). Considering the prominent self-assembly ability of the as-prepared $REPO_4$ nanocrystals, they are expected to have potential in constructing future self-assembled nanodevices.

5. Photoluminescence Properties of the Doped $REPO_4$ Nanocrystals. Rare-earth phosphates have been shown to be a useful host lattice for other lanthanide ions, producing phosphors emitting a variety of colors.[4] In this paper, a systematic study of the optical behavior of RE^{3+}-doped $REPO_4$ nanocrystals is reported. Figure 9a shows the room-temperature excitation and emission spectra of diverse shaped $La_{0.4}Ce_{0.45}Tb_{0.15}PO_4$ nanocrystals redispersed in cyclohexane. These transparent dispersions show an intensive green emission upon excitation with UV light (Figure 9d). A UV excitation of Ce^{3+} occurs through a $4f^1 \rightarrow 4f^05d^1$ transition. After an energy transfer from Ce^{3+} to Tb^{3+}, a Tb^{3+} emission of green light resulting from $^5D_4 \rightarrow {}^7F_J$ relaxation takes place.[4a,6d−f,8] As shown in Figure 9a, the luminescence spectra of monodisperse $La_{0.4}Ce_{0.45}Tb_{0.15}PO_4$ nanocrystals with different morphologies are quite similar and showed no significant difference from that of the bulk material.[9] On UV excitation of the cerium absorption band, in comparison with that of an ethanol (spectroscopic grade) solution of rhodamine 6G (Lambda Physics, laser grade) under identical optical density at the same wavelength, quantum yields (QYs) of 50, 47, 45, and 50% are obtained for the terbium emission of $LaPO_4$:Ce,Tb polyhedra, quasirods, rods, and wormlike wire dispersion, respectively.[5c,8] However, the QYs of the products obtained from DA/OM and HA/OM are only 30 and 15%, respectively. It is well-known that energy transfer to the surface through adjacent dopant and the quench of the surface dopant ions are two important factors lowering the QY. As the steric hindrance of DA and HA is weak, the nanocrystals obtained from DA/OM and HA/OM did not bear the risks of colloidal collapse and agglomeration, which

(9) (a) Smets, B. M. J. *Mater. Chem. Phys.* **1987**, *16*, 283. (b) Bourcet, J.-C.; Fong, F. K. *J. Chem. Phys.* **1974**, *60*, 34. (c) van Schaik, W.; Lizzo, S.; Smit, W.; Blasse, G. *J. Electrochem. Soc.* **1993**, *140*, 216. (d) Blasse, G.; Grabmaier, B. C. *Luminescent Materials*; Springer: Berlin, 1994. (e) Frey, S. T.; De Horrocks, W. *Inorg. Chem.* **1991**, *30*, 1073.

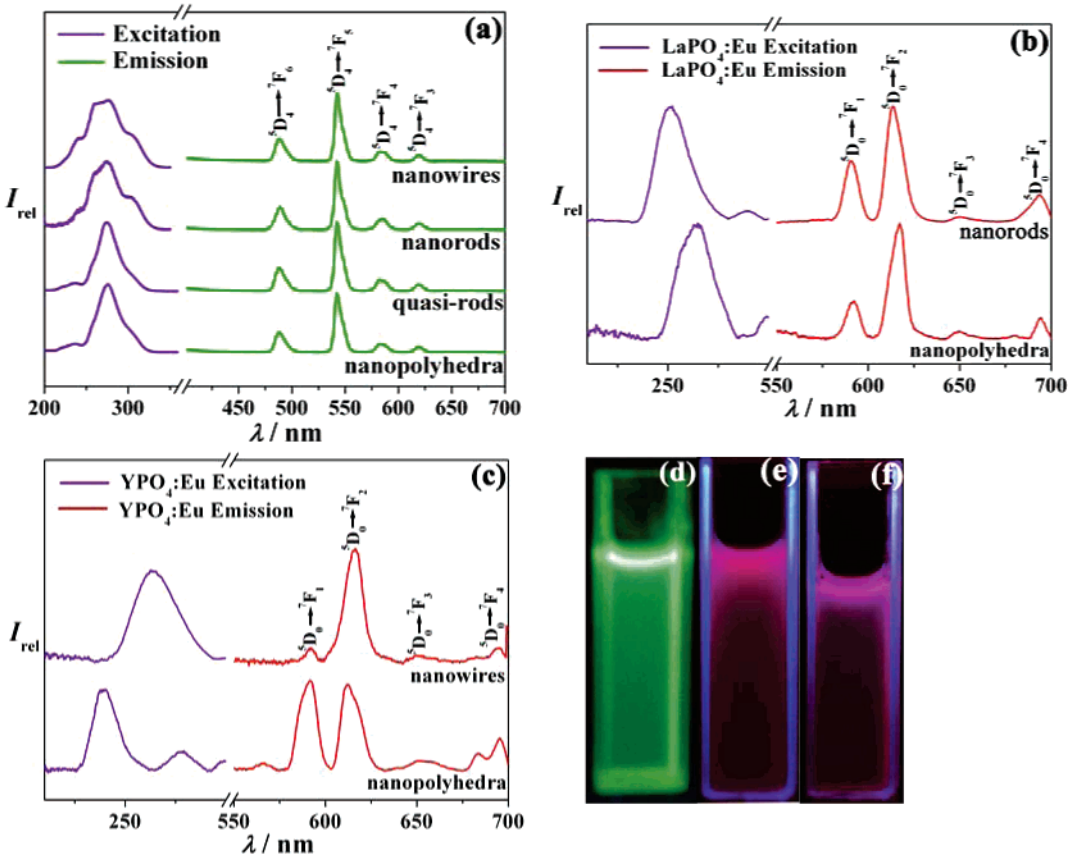

Figure 9. Room-temperature excitation and emission spectra of (a) $La_{0.4}Ce_{0.45}Tb_{0.15}PO_4$ polyhedra, quasirods, rods, and wormlike wires ($\lambda_{ex} = 272$ nm and $\lambda_{em} = 542$ nm), (b) $La_{0.95}Eu_{0.05}PO_4$ polyhedra and rods, and (c) $Y_{0.95}Eu_{0.05}PO_4$ polyhedra and wires. The fluorescence photographs of (d) $La_{0.4}Ce_{0.45}Tb_{0.15}PO_4$ nanopolyhedra, (e) $La_{0.95}Eu_{0.05}PO_4$ nanopolyhedra, and (f) $Y_{0.95}Eu_{0.05}PO_4$ nanowires dispersed in cyclohexane at a concentration of 2 wt % under $\lambda_{ex} = 254$ nm.

resulted in a severe surface damage. Therefore, their QYs are low.

Room-temperature excitation and emission spectra of $La_{0.95}Eu_{0.05}PO_4$ nanopolyhedra and nanorods are presented in Figure 9b. In the excitation spectrum of monoclinic $LaPO_4$:Eu nanorods, the broad band centered at 252 nm is attributed to a charge-transfer transition, which occurs by electron delocalization from the filled 2p shell of the O^{2-} to the partially filled 4 f shell of Eu^{3+}. The position of the charge-transfer band (CTB) observed for these $LaPO_4$:Eu nanorods is similar to the case of bulk $LaPO_4$:Eu (253 nm)[10a] and the $LaPO_4$:Eu nanorods acquired by hydrothermal treatment,[6a,c] indicating a similar local environment of the Eu^{3+} ions in the host lattices. However, an obvious shift of the CTB is observed for the 3.3 nm $LaPO_4$:Eu nanopolyhedra, with the maximum appearing at 264 nm. It is well-known that the CTB position depends on the Eu−O bond length: the longer the Eu−O bond length, the longer wavelength of the CTB.[6a,10b,c] Therefore, the nearly 10 nm red shift of the $LaPO_4$:Eu nanopolyhedra indicates that the average Eu−O bond distance is somewhat longer in $LaPO_4$:Eu nanopolyhedra than in $LaPO_4$:Eu nanorods, which agrees well with the decreased cell volume from the nanopolyhedra (311.1 Å^3) to the nanorods (306.0 Å^3). The emission spectra of the monazite $LaPO_4$:Eu nanorods and nanopolyhedra are described by the $^5D_0 \rightarrow {}^7F_J$ line emissions ($J = 0$, 1, 2, 3, and 4) of the Eu^{3+} ion. The orange-red emission lines at around 610 nm originating from the electric dipole transition $^5D_0 \rightarrow {}^7F_2$ are the dominant bands for both $LaPO_4$:Eu nanorods and nanopolyhedra. It is well-known that the $^5D_0 \rightarrow {}^7F_2$ transition is more sensitive to the local symmetry than the $^5D_0 \rightarrow {}^7F_1$ transition; when the size of the nanocrystals decreased, the ratio of surface Eu^{3+} ions increased and therefore, the symmetry around the Eu^{3+} ions decreases, leading to enhancement of the $^5D_0 \rightarrow {}^7F_2$ transition.[3f,4a,b] As a result, the ratio of I_{610}/I_{590} varied, which is 2.2 for the $LaPO_4$:Eu nanorods and 3.3 for the 3.3 nm $LaPO_4$:Eu nanopolyhedra (Figure 9b).

Figure 9c depicts the excitation and emission spectra of tetragonal $Y_{0.95}Eu_{0.05}PO_4$ nonuniform polyhedra and ultrathin nanowires. It can be seen that the position of the CTB in YPO_4:Eu nanopolyhedra is 239 nm, showing a notable blue shift compared with its position in the monoclinic $LaPO_4$:Eu, revealing that the RE−O bond distance is much shorter in tetragonal YPO_4:Eu than in monoclinic $LaPO_4$:Eu.[6a,c] However, the position of the CTB in YPO_4:Eu ultrathin nanowires is 263 nm, which is similar to the position in the monoclinic $LaPO_4$:Eu nanopolyhedra. Noticeably, because the YPO_4:Eu nanowires with a width of 1.4 nm have a large fraction of surface Eu atoms, the I_{610}/I_{590} of these nanowires is as high as 16, much higher than that of the nonuniform

(10) (a) Yu, M.; Lin, J.; Fu, J.; Zhang, H. J.; Han, Y. C. *J. Mater. Chem.* **2003**, *13*, 1413. (b) Hoefdraad, H. E. *J. Solid State Chem.* **1975**, *15*, 175. (c) Tao, Y.; Zhao, G.; Ju, X.; Shao, X.; Zhang, W.; Xia, S. *Mater. Lett.* **1996**, *28*, 17.

YPO_4:Eu nanoparticles (20−50 nm, $I_{610}/I_{590} = 1.0$) (Figure 9c).

Comparing the PL behavior of these two kinds of Eu^{3+} doped nanocrystals, we can see that for both the monoclinic and tetragonal orthophosphate host, the excitation and emission spectra vary with the crystallite size. When the size of the $REPO_4$ nanocrystals decreases, the positions of the CTB bands show red shift, indicating that the RE−O bond distance becomes longer as the particle size shrinks. Moreover, we find that when the size of the $REPO_4$ nanocrystals become ultra small (3.3 nm monoclinic $LaPO_4$:Eu nanopolyhedra, 1.4 nm width tetragonal YPO_4:Eu nanowires), the positions of the CTB bands are very similar (264 nm for $LaPO_4$:Eu nanopolyhedra and 263 nm for YPO_4:Eu nanowires). Therefore, we suggested that when the size of the $REPO_4$ nanocrystals decreased enough, the RE−O bond distance in the $REPO_4$ would be similar. Also, the decrease in the nanocrystal size of the $REPO_4$ leads to the increase in I_{610}/I_{590}, revealing that the ratio of surface Eu^{3+} ions increase with decreasing the particle size. In particular, the as-obtained monodisperse $LaPO_4$:Eu nanopolyhedra, nanorods and YPO_4:Eu nanowires show intensive red emissions upon excitation with UV light (images e and f in Figure 9), and the QYs are 46, 42, and 40%, respectively, which are much higher than those of the nonuniform samples (QY = 10%). These results all show that the monodisperse $LaPO_4$:Ce,Tb, $LaPO_4$:Eu, and YPO_4:Eu nanocrystals with diverse shapes obtained from OA/OM and LA/OM are of high quality in terms of few lattice defects and less surface damage, which makes them promising nanocrystalline phosphors for future applications.

Conclusions

Through tuning the crystal growth kinetics with designed chemical reactions, we have found that the LAER strategy demonstrated in this work is an effective, facile, and economical approach toward the synthesis of high-quality $REPO_4$ nanocrystals with diverse shapes. 0D nanopolyhedra and 1D nanorods and nanowires can be controllably obtained by simply changing the alkyl-chain length of the capping ligands. The as-synthesized doped $REPO_4$ nanopolyhedra, quasinanorods, nanorods, and nanowires show intensive green and red emission under UV excitation with high quantum yields. The luminescent nanocrystals can be orderly aligned on the copper substrate to form 2D and 3D nanoarrays on a large area. Moreover, this LAER synthetic strategy is extendable to many other inorganic salt nanocrystals such as YVO_4, $NaYF_4$, sulfides, and II−VI group semiconductors. This research has opened new opportunities not only in fabricating high-quality inorganic nanocrystals by turning the reactivity of chemical reactions, and in developing advanced functional materials and devices by tailoring the self-assembled pattern of nanobuilding blocks with the so-called bottom up nanotechnology.

Acknowledgment. We gratefully acknowledge the financial aid from the MOST of China (Grant 2006CB601104), the NSFC (Grants 20571003, 20221101, and 20423005), and the Research Fund for the Doctoral Program of Higher Education of the MOE of China (Grant 20060001027).

Supporting Information Available: More results obtained by means of XRD, TEM, EDAX, and FTIR for $REPO_4$, YVO_4, and $NaYF_4$ nanocrystals (PDF). This material is available free of charge via the Internet at http://pubs.acs.org.

CM071073L